Validation of MODIS F_{PAR} Products in Boreal Forests of Alaska

Daniel C. Steinberg, Scott J. Goetz, and Edward J. Hyer

***Abstract*—Moderate Resolution Imaging Spectroradiometer (MODIS) fraction of photosynthetically active radiation absorbed by vegetation (F_{PAR}) products covering the boreal forest of interior Alaska were analyzed and compared with field measurements of canopy light harvesting over a multiyear period (2001 to 2004), as well as to high-resolution F_{PAR} maps derived from IKONOS and Landsat ETM+ imagery. The spatial variability of F_{PAR} within the MODIS products was examined by incorporating the field measurements and aggregating the high-resolution F_{PAR} maps to the MODIS scale. Characterization of the temporal accuracy of the MODIS F_{PAR} products was conducted through comparisons with continuously operating canopy light interception measurements. The MODIS product tended to overestimate F_{PAR} relative to both ground-based measurements and Landsat-derived estimates of F_{PAR}, particularly in the more sparsely vegetated burn scars on which we focus related research, but adequately captured seasonal variability associated with vegetation phenology. A combination of canopy closure and ground cover vegetation was identified as the source of most of the discrepancies between the MODIS estimated and field measured F_{PAR} values. Neither the field measurements nor the high resolution image F_{PAR} maps based on the field measurements characterized the light environment of the ground cover vegetation (i.e., <10 cm height); thus, absolute validation of the MODIS products was incomplete—despite the extensive spatial and temporal characterization of F_{PAR} dynamics in the study region. We discuss these results, explore some other possible sources for observed differences between the MODIS, field, and high-resolution F_{PAR} maps, and consider possible ways to address these issues in future work.**

***Index Terms*—Boreal, fraction of photosynthetically active radiation absorbed by vegetation (F_{PAR}), Moderate Resolution Imaging Spectroradiometer (MODIS), satellite remote sensing, validation.**

I. Introduction

THE fraction of photosynthetically active radiation absorbed by vegetation (F_{PAR}) is a key biophysical property from which a number of ecosystem properties can be estimated. F_{PAR} is used, for example, to monitor changes in vegetation properties and their impact on models of net primary production, eco-hydrology, and energy exchange [1]–[3]. It is, therefore, useful to have global measurements of F_{PAR} with a frequent periodicity in order to support regional to global modeling and monitoring efforts.

The Moderate Resolution Imaging Spectroradiometer (MODIS) F_{PAR} product [4] provides global 1-km resolution images at eight-day intervals. Validation activities have been initiated to assess product accuracy through comparisons with high-resolution satellite imagery and field measurements [5]–[7]. These validation efforts help to reveal uncertainties in the satellite estimates and provide a basis for improving the MODIS algorithms. Assessments need to be carried out over a range of conditions in order to examine the performance of the product algorithm over different vegetation and ground cover types [4].

Recent validation efforts of the MODIS LAI/F_{PAR} products have focused primarily on the assessment of LAI. To date, only two studies have closely examined the accuracy of the F_{PAR} product in relation to ground based or high resolution estimates, and both have been carried out at research sites in Africa: one in a semi-arid grassland [8], and another in a Kalahari woodland [9]. Extension of validation efforts to other biomes is needed to gain a more comprehensive assessment of the F_{PAR} products. Reference [7] reviews the results of these studies in greater detail.

In this study, we assessed the accuracy of the MODIS F_{PAR} product in the boreal forest of interior Alaska. The boreal region was recently highlighted as the most rapidly changing environment on the planet [10]. Release of the suite of MODIS vegetation products (see [11]) presents an opportunity to monitor changes in the boreal biome, but utility of the products depends on their accuracy and consistency. The MODIS F_{PAR} products will be of particular importance for carbon models exploring the effects of fire disturbance and regrowth on carbon cycling in the region [12], [13].

We examined the accuracy of the MODIS F_{PAR} product using high-resolution satellite imagery in conjunction with field-based measurements of canopy light harvesting over a multiyear period at a range of sites, including several in various stages of regrowth following fire disturbance, a common occurrence in the region. Spatial variability of the MODIS product was examined through comparisons with high resolution F_{PAR} maps derived from empirical relationships between Landsat ETM+ imagery and hand-held measurements of canopy light interception. Temporal variability was examined using direct comparisons to continuous automated measurements of light interception throughout the growing seasons of 2002, 2003, and 2004.

Manuscript received January 3, 2005; revised April 15, 2005. This work was supported in part by by the National Oceanographic and Atmospheric Administration Carbon Cycle Science Program (NA17RJ1223) and in part by the NASA ADRO program (NAG510097).

D. C. Steinberg and S. J. Goetz are with the The Woods Hole Research Center, Woods Hole, MA 02543 USA (e-mail: sgoetz@whrc.org).

E. J. Hyer is with the Department of Geography, University of Maryland, College Park, MD 20742 USA.

Digital Object Identifier 10.1109/TGRS.2005.862266

II. Study Area

Field measurements were conducted in the Delta Junction region of Alaska, located approximately 150 miles Southeast of Fairbanks, AK, in the Upper Tanana River Valley (Fig. 1). Black spruce (*Picea mariana*), quaking aspen (*Populus tremuloides*), paper birch (*Betula papyrifera*), and various willow (*Salix*) species dominate the vegetation of the region. A "chronosequence" of fires from 1954, 1987, 1994, 1999, and 2004 encompass a broad range of age classes, basal area, stem density, and canopy closure, each influenced by the interplay of burn severity, topography, time of fire during the growing season, and edaphic conditions [14], [15].

The 1999 Donnelly Flats burn consumed 7575 hectares and left most of the area with standing, charred black spruce snags. The 1994 Hajdukovich Creek fire burned 8897 ha, leaving most of the area with downed black spruce snags [Fig. 2(a)]. The 1987 Fort Greeley fire burned 20 009 ha from which a combination of mostly aspen and spruce has regrown [Fig. 2(b)]. Tree heights of the regrowth ranged from 1–3 m in the 1994 burn to 4–6 m in the 1987 burn. Ground cover in the region is relatively heterogeneous due to the high frequency of fire disturbance; however, mosses and lichens dominate older sites, which have recovered from the initial charring following burns. More severely burned sites also tend to have less organic soil, tend to be less mesic, and ground cover vegetation less abundant. However, due to variation in fire severity and edaphic conditions within a single burn, there are no easily definable trends between fire history and ground cover.

III. Methods and Data Sets

Individual handheld measurements of canopy light interception were collected between June 4, 2001 and August 12, 2001, at sites within the Delta Junction study area [16]. Automated continuous measurements of light interception were collected throughout the growing seasons of 2002, 2003, and 2004. The site selection and measurements are described in more detail below.

A. Field Sampling Design

Two types of sites were established in the study area. Ten sites were of a "grid" design consisting of two parallel transects within a 200 × 200 m (40 000 m^2) area, where each transect was 150 m in length. At 50-m intervals along each transect, perpendicular 10-m line transects were sampled at 1 m intervals (Fig. 3.). Another 28 sites were established within 150 × 150 m (22 250 m^2) areas, each bisected by a single transect of 100 m in length with ten plots set at 10-m intervals. Landsat imagery was used in conjunction with field surveys to ensure that selected sites exhibited relatively homogeneous canopy cover.

The sites were distributed across the study region and stratified by areas that had burned in 1956, 1987, 1994, and 1999. One grid site was established in the 1987 burn, two each in the 1956 and 1999 burns, and three in the 1994 burn. In addition, two grid sites were established in unburned areas representative of the pre-burn Donnelly Flats vegetation (i.e., mature upland and lowland black spruce). The various sites were selected to represent a range of site conditions, stand age, density, and composition (see Fig. 2).

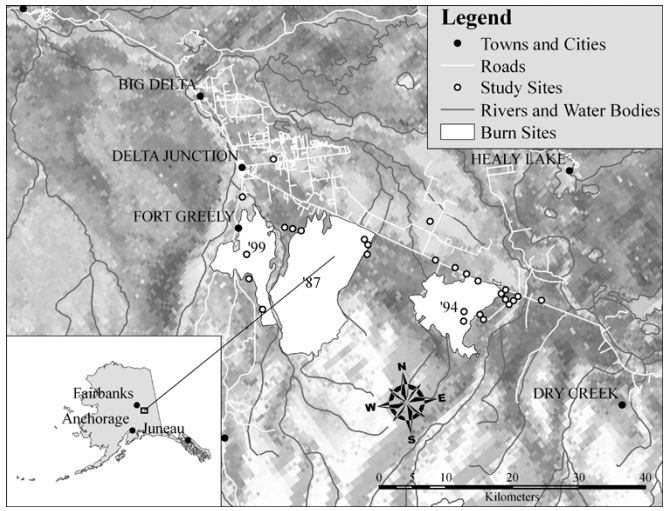

Fig. 1. Study area in interior Alaska. Individual study and burn sites are shown.

1) Indirect Measurements of Canopy F_{PAR}*:* Indirect estimates of canopy F_{PAR} [17] were calculated using measurements of canopy light interception made at each site using a Decagon "AccuPAR" ceptometer (*Decagon Devices, Inc.)*. The ceptometer measures incident radiation in the PAR wavelengths (400–700 nm), from which estimates of canopy transmission (τ) are made through simple ratioing of above and below-canopy measurements. Reference [16] describes the measurements and related sensitivity analyses in greater detail. The responses of the 80 photodiodes were averaged for each instantaneous measurement, of which we made 20 along each transect (2 in opposite directions at 10-m intervals) and 160 at each grid site (i.e., eight transects of 10-m each with a 1-m sampling interval). Measurements were made at 10 cm in height above the surface in order to avoid interference by low-lying vegetation. Due to the height of our measurements, ground cover light interception was not included in our final values. Above (outside) canopy measurements were made at the beginning and end of each transect or grid site and in canopy gaps when available. F_{PAR} values, derived from the ceptometer measurements as $1 - \tau$, were subsequently used to determine relationships between IKONOS and Landsat NDVI and F_{PAR} (discussed further in Section III-A4), from which high-resolution F_{PAR} maps were developed.

2) Par Cell Phenology: Automated continuous measurements of incident and intercepted radiation were made using a custom set of solar cells, produced by Solems Industrie (France), which measured both incident PAR and total short-wave radiation. A total of 94 cells, laminated with isotropic filters, were strung together in sets of ten cells, arranged as five pairs per string. The nine strings were divided into two sets, one with 50 cells and one with 40 cells. Each cell was placed on a 10-cm post in order to minimize interference from low-lying vegetation. The four remaining cells were reserved for above-canopy measurements of incident PAR (two accompanying each set). These above canopy measurements were augmented with four calibrated LICOR 190SA and

Fig. 2. Images displaying stand and ground conditions in the (a) 1994 and (b) 1987 burn sites, and in (c) the unburned spruce site.

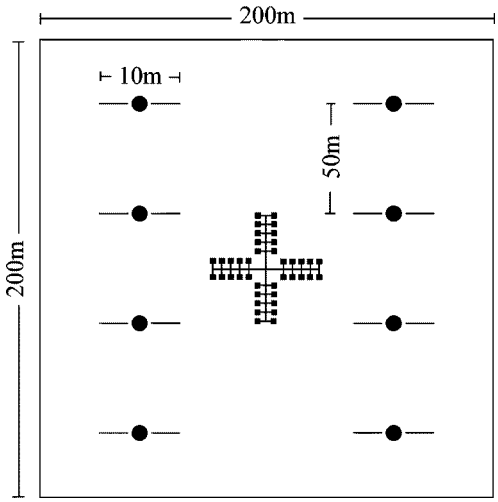

Fig. 3. Schematic illustrating the sampling design of a "grid site." Solid dots indicate the location of each 10-m line transect which were sampled at 1-m intervals. A PAR cell array is shown at the center of the grid indicating the typical orientation and location of the array.

Apogee PAR sensors. Each array, when deployed, covered an area of approximately 400 m^2, characterizing an area at least comparable in size to a Landsat pixel (900 m^2).

The two cell arrays were operated at five different sites over three years (2002–2004), where each array was associated with one of the ten grid sites described earlier. Arrays were strategically located in areas representative of the vegetation of the associated study site. In order to capture the phenological and seasonal dynamics of light interception, arrays were deployed in early spring and run continuously throughout the growing season. In 2002, arrays were deployed in the 1987 and 1994 burns, at the 1987a and 1994b sites [Fig. 2(a) and (b)]. The following year (2003), one of the two arrays was moved to the unburned spruce site [Fig. 2(c)], while the other remained in the 1987 burn, but was relocated within the burn, to the 1987b site. This allowed us to characterize the light harvesting dynamics of an evergreen site (unburned spruce) while also establishing a multiyear record at the 1987 burn site. Movement of the array within the 1987 burn allowed for a more comprehensive characterization of F_{PAR} dynamics. In 2004, the array from the unburned spruce site was returned to the 1994 burn and deployed at the 1994b site. Again, collection of data from multiple sites within each burn allowed us to more comprehensively characterize light interception of the region. The 1999 burn was not measured with the PAR cell arrays, because the little vegetation that had re-established was dominated by grasses.

Minimum and maximum measurements for each string of the arrays were recorded every 15 s on Campbell CR10X data loggers, and subsequently averaged every 10 min. PAR cell responses (millivolts) were converted to energy fluxes (μmol $m^{-2}s^{-1}$), using the calibrated Licor and Apogee quantum sensors. The PAR cell arrays were calibrated at the beginning and end of each measurement season in order to account for any drift over the observational period.

The data from each string were processed and filtered to remove values where:

1) PAR_{above} (above canopy PAR) $<$ PAR_{below}(below canopy PAR), or
2) $PAR_{below} < 0$.

As with the handheld measurements, F_{PAR} values for each string were calculated as $1 - \tau$.

Daily F_{PAR} for each array was calculated as the mean F_{PAR} value from all strings within an hour of the MODIS Terra overpass (between 11:30 and 13:30 local time). Mean daily F_{PAR} values were then used to construct a time series of daily F_{PAR} at each site location. Data were also averaged to eight-day values

and subsequently compared with the MODIS eight-day F_{PAR} product.

3) MODIS Data: The MODIS LAI/F_{PAR} product (MOD15A2) is produced globally at 1-km spatial resolution and is composited over an eight-day period based on the maximum F_{PAR} value [4]. The products are projected on a World Sinusoidal 10°grid, where the globe is divided into individual $\sim 1200 \times 1200$ km tiles for processing and distribution purposes (36 tiles along the east-west axis, and 18 tiles along the north-south axis). Each tile contains LAI, F_{PAR}, and two quality assessment (QA) layers, which contain information on the quality of individual pixel estimates, cloud contamination, and algorithm use.

The MODIS LAI/F_{PAR} algorithm uses a look-up-table (LUT) approach to calculate the most probable values of F_{PAR} and LAI for each pixel. It uses as inputs up to seven bi-directional Reflectance Distribution Functions (BRDFs) adjusted reflectances, sun-view geometries, and the MODIS Land Cover type product (MOD12Q1). The algorithm LUTs are based on canopy reflectances over a range of canopy structure and ground cover conditions typical of a given biome type, and are compared with observed MODIS reflectance product values (MOD09) [18]. For cases where the difference between observed and modeled reflectances is less than the uncertainty of the observed reflectance values, canopy structural variables used as inputs to the model are taken as possible solutions for F_{PAR} and LAI [18], [19]. The retrieved F_{PAR} value is calculated as the mean of all possible solutions. If a unique solution is found, this value is reported as the retrieval. In cases where no solutions are found, a back-up algorithm is used to predict F_{PAR} based on empirical relationships of F_{PAR} to MODIS vegetation index products [4]. This latter approach is comparable to our derivation of F_{PAR} maps from the Landsat imagery and field measurements.

The MODIS F_{PAR} products were acquired for our study area for the years 2001–2004. Using the quality assessment layers, F_{PAR} data were filtered using two different quality control schemes. First, all tiles from 2002–2004 were screened such that only pixels with the "best possible" designation under the QA description were retained for each tile (Table I). This corresponds to pixels that were retrieved using the primary F_{PAR} algorithm during minimal cloud cover. We conducted additional screening to retain pixels with the "best possible," or "ok, but not the best" designation under the QA description. This included pixels retrieved by both the main and back-up algorithm, and excluded pixels which were not produced due to cloud cover, snow, or other factors (Fig. 4).

Following the data quality screening, a time series of MODIS F_{PAR} at each study site was constructed and compared with our *in situ* F_{PAR} measurements collected using the PAR cell arrays. MODIS F_{PAR} values from the single pixel overlying each PAR cell array were extracted from each quality filtered eight-day composite throughout the study period. These values were then plotted through time in order to create a continuous time series of MODIS F_{PAR}. MODIS radiometric data were extracted from the original World Sinusoidal projection, minimizing resampling of the MODIS data.

TABLE I
MODIS F_{PAR} QUALITY CONTROL DEFINITIONS FOR COLLECTION 4 DATA

FPAR Quality Control Definition for collection 4 data (v4.*)		
Bitfield	Binary, Decimal Values	Description of Bitfield(s)
MODLAND {0,1}	00=0	Best possible
	01=1	Ok, but not the best
	10=2	Not produced, due to cloud
	11=3	Not produced, due to other reasons
DEAD-DETECTOR {2}	0=0	Detectors OK for up to 50% of channels 1,2
	1=1	Dead detectors forced >50% adjacent retrievals
CLOUDSTATE {3,4}	00=0	Significant clouds NOT present
	01=1	Significant clouds WERE present
	10=2	Mixed cloud present on pixel
	11=3	Cloud state not defined, assumed clear
SCF_QC {5,6,7}	000=0	Main radiative transfer (RT) method used with the best possible results
	001=1	Main RT method used with saturation
	010=2	Main RT method failed due to geometry problems, empirical method used
	011=3	Main RT method failed due to problems other than geometry, empirical method used
	100=4	Couldn't retrieve pixel

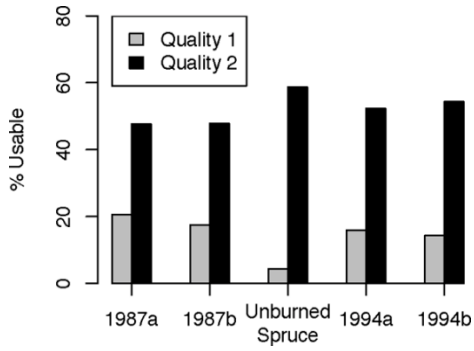

Fig. 4. Graph depicting the percentage of available pixels that are retained throughout the study year, under quality filtering schemes 1 and 2. Retaining only pixels with the "best possible" quality control definition drastically limits the number of usable pixels.

Individual F_{PAR} measurements collected with the AccuPAR ceptometer were compared with MODIS pixels using a "MODIS grid," displaying MODIS pixel edges overlaid on a map of our field F_{PAR} measurements. All screened measurements within the boundary of a single pixel were averaged and compared to the value of the overlying MODIS pixel. MODIS pixels were extracted from the composite image, which had an acquisition date closest in time to the sampling date of the field measurement. Pixels from these composites were occasionally missing due to data quality screening, and were not included in the analysis.

In addition to the MODIS F_{PAR} product, the MODIS Land Cover (MOD12Q1) product [20], and the MODIS eight-day 250-m NDVI product (MOD13Q1) [21] were acquired for the study area. The MODIS land cover product is one of the inputs into the MODIS LAI/F_{PAR} algorithm; as a result, biome misclassification in the land cover product can introduce errors into the MODIS F_{PAR} product [22], [23]. In order to assess the influence of these errors on MODIS F_{PAR} retrievals, land cover statistics were compiled over the 1999, 1994, and 1987 burns (Table II) and assessed based on field knowledge of local land cover. The MODIS NDVI product was also examined to assess

TABLE II
PERCENTAGE COVERAGE OF EACH BIOMETYPE OVER THE 1987, 1994, AND 1999 BURNS

% Coverage over three burns			
Burn Year:	1987	1994	1999
Water	0.0	0.0	0.0
Grasses/Cereal Crops	4.2	0.0	0.0
Shrubs	23.6	22.4	22.6
Broadleaf Crops	0.0	0.0	0.0
Savanna	44.7	46.9	38.1
Broadleaf Forest	1.7	0.0	3.6
Needleleaf Forest	25.7	30.6	33.3
Total Forested	27.4	30.6	36.9
Unvegetated	0.0	0.0	2.4
Total Area:	100.000	100.000	100.000

uncertainties in the F_{PAR} comparisons across multiple scales, i.e., using Landsat and IKONOS imagery, and to discern the effect of spectral mixing at MODIS resolution.

4) ETM+ Processing and F_{PAR} *Maps:* Landsat ETM+ scenes available for relatively cloud-free periods between 2001–2004 were acquired as level-1b products. An orthorectified Landsat-7 Earthsat ETM scene, acquired on September 15, 1999, was used as the base image to which all other acquisitions were georeferenced. Control points were also acquired in the study area using GPS to increase the precision of the georectification. The calibrated radiances were converted to top-of-atmosphere (TOA) reflectances using in-band spectral solar irradiances and a solar geometry model to correct for Earth-Sun distance and solar zenith angle variations [24]. No atmospheric measurements were available for absolute atmospheric correction but the images were collected under clear conditions, and were adequate for our purposes (i.e., spatially extending the field F_{PAR} measurements).

F_{PAR} maps of 30-m resolution were derived from the georeferenced TOA ETM scenes using simple linear regression relationships with our field-based measurements of F_{PAR}. A Landsat grid was overlaid on a map of the ceptometer measurements, and the mean of all F_{PAR} measurements within the boundary of a single grid cell were plotted against the NDVI of the overlying Landsat pixel. Regression models were developed on an individual scene basis, and stratified into deciduous versus evergreen sites. We found the best fit using all available data across scene dates ($N = 94$, $R = 0.79$, $p < 0.0001$), and based our empirical F_{PAR} estimates on the resulting model ($F_{PAR} = 1.26\ NDVI + 0.011$). This single regression was then applied to the each Landsat scene in order to convert NDVI values to F_{PAR} [Fig. 5(b)]. A 2000-km^2 subset of the study region was extracted from each ETM F_{PAR} image, and the images were degraded to the exact MODIS pixel size, by averaging all fine resolution F_{PAR} values within each MODIS pixel ($N = 926$). Quality-controlled MODIS scenes were reprojected into the Albers Equal Area projection in order to correspond to the ETM imagery, and a subset of the study region was then extracted from the MODIS composite. The MODIS scale ETM subsets were subsequently compared to MODIS F_{PAR} subsets on a per-pixel basis. Acquisition dates of MODIS and ETM imagery were matched as best as possible, and no date differed by more than four days.

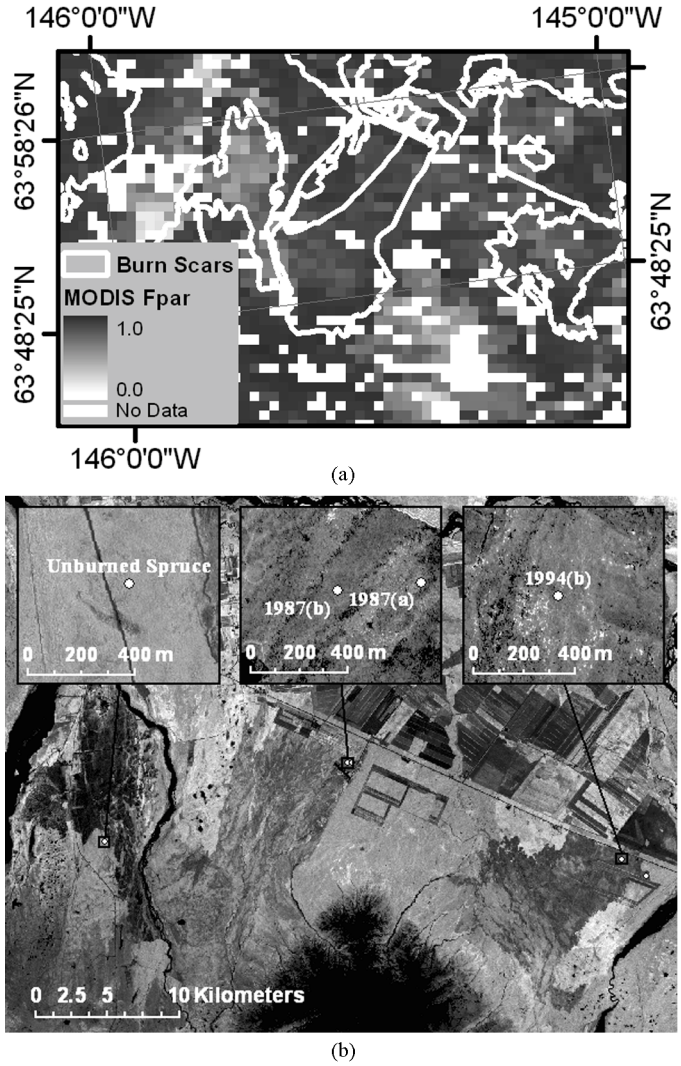

Fig. 5. (a) Subset of a quality-filtered MODIS F_{PAR} tile (July 21, 2002) showing the study region. Missing pixels within this example are shown in white. (b) Landsat F_{PAR} image (acquired June 2, 2001) of the study region. Image insets show IKONOS F_{PAR} centered on three of the study sites. White dots indicate the location of study sites (PAR cell locations) within each of the burns. Dates of acquisitions of IKONOS imagery from left to right: May 26, 2001, July 18, 2001, and July 18, 2001.

In addition to the F_{PAR} maps, 30-m NDVI images were calculated from the georeferenced TOA ETM scenes, and a subset of the study region was extracted from each Landsat NDVI image. As with F_{PAR}, the images were subsequently degraded to 250-m resolution in order to correspond to the MODIS NDVI product resolution. Aggregation of the fine resolution Landsat data was carried out by averaging all high-resolution pixels within the boundaries of a single MODIS pixel. MODIS NDVI scenes were reprojected into the Albers Equal Area projection, and a subset of the study region was extracted. The 250-m Landsat NDVI subsets were then compared to the MODIS NDVI subsets on a per pixel basis.

IV. RESULTS

Filtering the MODIS F_{PAR} product results using the quality flags reduced, as expected, the number of usable pixels per

image to a fraction of those possible (Fig. 4). Relaxing the filtering to include second tier quality flags ("OK but not the best") increased the number of usable pixels and allowed us to produce and work with MODIS $\mathrm{F_{PAR}}$ maps covering a reasonable extent of the study area through time. None of the third or fourth tier data were used, and only second tier data unaffected by clouds, snow cover, detector or sensor problems were included (see Table I). These derived MODIS products were used in the analyses that follow.

A. Comparisons With Field Measurements

In situ $\mathrm{F_{PAR}}$ measurements acquired with the Decagon Ceptometer ranged from 0.18 to 0.95 over our set of 30 sampling sites. The corresponding MODIS values ranged from 0.46 to 0.93, and were moderately well correlated with the field estimates (Fig. 6). The MODIS $\mathrm{F_{PAR}}$ values were less variable and overestimated relative to our ground measurements, particularly in areas with lower field measured $\mathrm{F_{PAR}}$ $(\mathrm{R} = 0.58, \mathrm{p} = 0.0006)$.

The 2002, 2003, and 2004 time series of PAR cell array measurements did not always capture the full extent of seasonal variation in $\mathrm{F_{PAR}}$ due to various quality control issues, but we were able to capture a range of continuous measurements available at a few other sites. Seasonal dynamics of $\mathrm{F_{PAR}}$ varied between sites due to differences in vegetation density, composition, and stand age. At the four deciduous sites [Fig. 7(a)–(d)], our *in situ* measurements display a typical $\mathrm{F_{PAR}}$ phenology where leaf-flush drives an increase in $\mathrm{F_{PAR}}$, reaching a maximum at mid-summer, and decreasing as leaf senescence ensues at the end of the season. In contrast, the mature spruce site exhibited the inverse of this seasonal pattern, where the beginning and end of season were marked by local maxima of $\mathrm{F_{PAR}}$ and the minimum was reached at mid-season [Fig. 7(e)].

The time series of MODIS $\mathrm{F_{PAR}}$ measurements compared with the *in situ* measurements (Fig. 7) indicate that the MODIS $\mathrm{F_{PAR}}$ retrievals tended to overestimate $\mathrm{F_{PAR}}$ relative to our ground-based measurements. At all five study sites, where the PAR cell arrays were operated, MODIS $\mathrm{F_{PAR}}$ values exceeded the observations, although the magnitude of the differences varied between sites and throughout the season (ranging from 0.05 to 0.4). With the exception of the 1994b site, the difference between field and MODIS estimates reached a maximum at or near mid-season ($\sim$day 195), and as the season progressed, MODIS $\mathrm{F_{PAR}}$ tended to converge with our *in situ* measurements. At the 1994b burn site, however, the maximum offset occurred during the green-up, and diminished throughout the season.

The strongest correlation between all seasonal MODIS and field-based measurements was observed at the 1987a site. The offset never exceeded 0.1 and typically averaged 0.05. At all four other sites, we found more pronounced differences, with the largest occurring at the 1994b site, where MODIS overestimated $\mathrm{F_{PAR}}$ by up to 0.4. Maximum differences observed at the 1987b burn, 1994a burn, and unburned spruce sites were 0.2, 0.25, and 0.3, respectively. Pearson correlation coefficients at the sites ranged from 0.93 at the 1987b site to 0.06 at the spruce site (Table III), although the low correlation at the latter was largely due to the limited seasonal variability

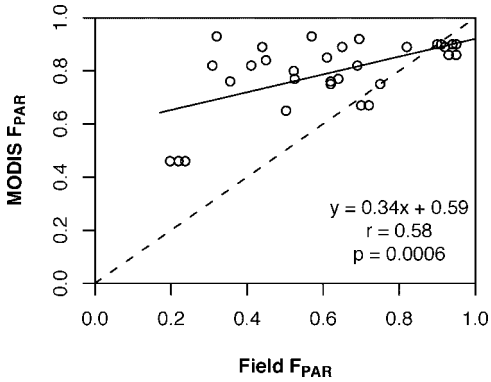

Fig. 6. Comparison of the MODIS F_{PAR} product to field measurements taken using a Decagon ceptometer.

of $\mathrm{F_{PAR}}$ at the site. The simple linear regression of eight-day MODIS $\mathrm{F_{PAR}}$ and eight-day averaged field $\mathrm{F_{PAR}}$ from all sites (Fig. 8) shows that the discrepancies between the MODIS $\mathrm{F_{PAR}}$ product and the PAR-cell array measurements are greater at lower $\mathrm{F_{PAR}}$ values and decrease with increasing magnitude of $\mathrm{F_{PAR}}$ $(\mathrm{y-intercept} = 0.54, \mathrm{R} = 0.391)$. The mean difference over all sites between MODIS and PAR-cell estimates is 0.16, indicating a mean offset of the same magnitude. Seasonal variation in $\mathrm{F_{PAR}}$ was reasonably well characterized by the MODIS product. The field and MODIS estimates follow similar green-up and senescence patterns throughout the growing season and display similar seasonal patterns of variation.

B. Comparisons With High Resolution $\mathrm{F_{PAR}}$ Maps

The Landsat-derived $\mathrm{F_{PAR}}$ image [Fig. 5(b)] captured a wide range of $\mathrm{F_{PAR}}$ across the study area. Direct comparison of the MODIS and Landsat $\mathrm{F_{PAR}}$ maps also indicated that the MODIS products overestimated $\mathrm{F_{PAR}}$, particularly in burned areas (Fig. 9). The offset between the MODIS and ETM products was approximately 0.2, which was similar to that observed between MODIS and the PAR cell arrays. Spatial variability in $\mathrm{F_{PAR}}$ captured in the resampled Landsat $\mathrm{F_{PAR}}$ was comparable to that in the MODIS product (Fig. 9), and we note that the largest disagreement between MODIS and aggregated Landsat pixels generally fell over sparsely vegetated areas, including recent burns.

Comparison of the MODIS 250 m NDVI product to aggregated Landsat NDVI revealed that MODIS NDVI, calculated from atmospherically corrected reflectances, was consistently higher than the Landsat NDVI [Fig. 10(a)], although the two were highly correlated $(\mathrm{r} = 0.83)$. The comparison of Landsat NDVI to aggregated IKONOS NDVI revealed that NDVI values calculated using Landsat TOA reflectances were consistently higher than IKONOS NDVI [Fig. 10(b)]. As with the MODIS-Landsat NDVI comparison, Landsat and IKONOS NDVIs were highly correlated $(\mathrm{r} = 0.90)$.

V. Discussion

The observed disparity between the averaged individual ceptometer measurements and the MODIS $\mathrm{F_{PAR}}$ estimates were at least partly due to differences in the spatial scale of the

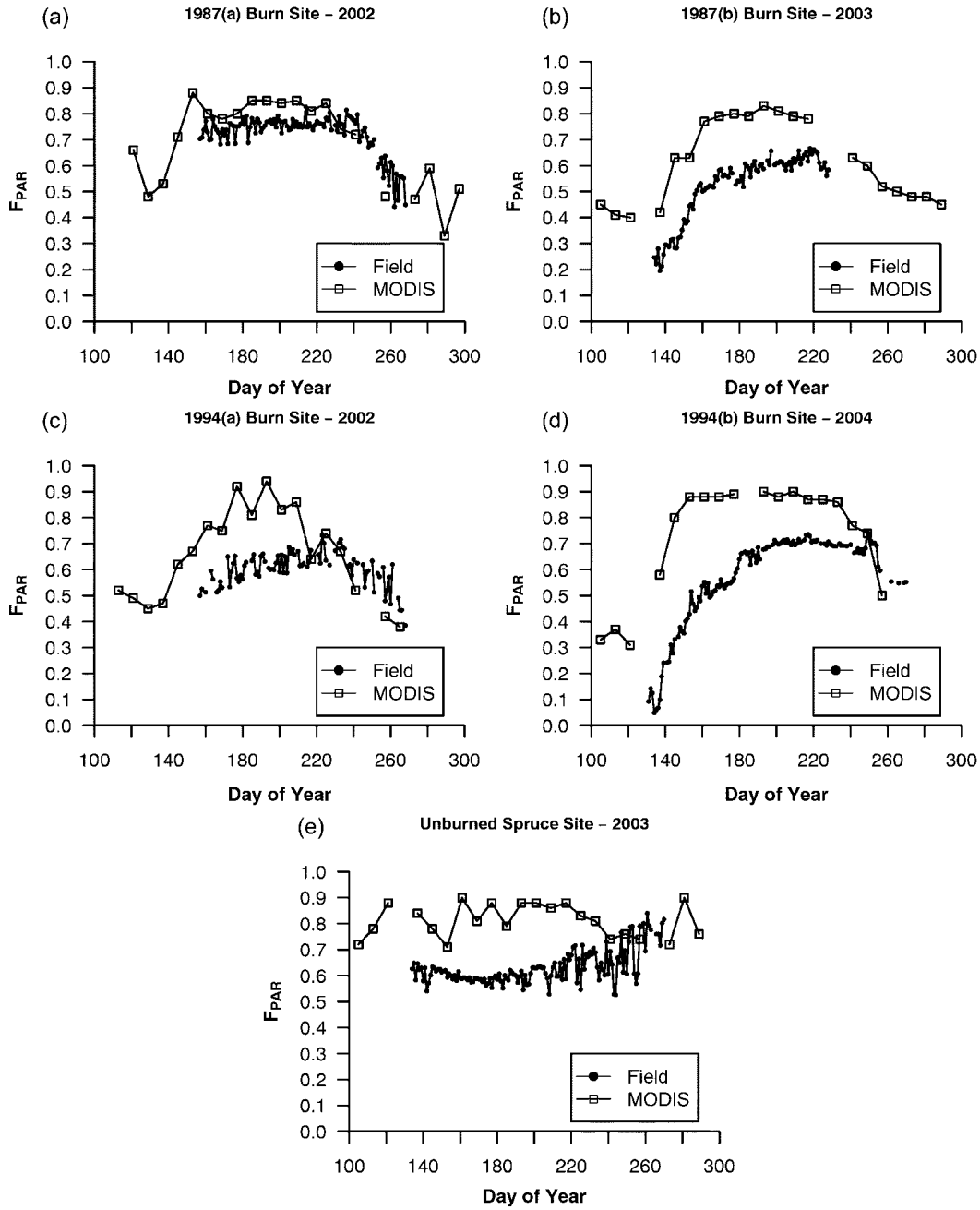

Fig. 7. Time series of PAR cell and MODIS eight-day F_{PAR} measurements. The study site where each time series was extracted from is indicated on the graph. Note that there are two different study sites within both the 1987 and 1994 burns.

field and satellite observations. Despite the acquisition of ceptometer measurements over relatively homogeneous areas and utilizing a sampling design to capture spatial variability, it was not possible to adequately characterize an area equivalent in size to a MODIS pixel with field measurements alone. Species composition, canopy density, and ground cover, vary greatly across the study region, and large differences in all exist across areas as small as 0.25 km^2. The ceptometer measurements were useful for capturing more local variability in canopy light harvesting and in permitting the development of finer resolution F_{PAR} maps from IKONOS and Landsat imagery [Fig. 5(b)].

Comparisons of the PAR cell array F_{PAR} measurements to MODIS F_{PAR} suggest that the MODIS product captured seasonal dynamics of F_{PAR} with reasonable accuracy, but tended

TABLE III
STATISTICS FROM THE REGRESSION ANALYSIS OF THE MODIS AND FIELD F_{PAR} TIME SERIES AT EACH STUDY SITE

Study Site	Sample Size (N)	P- value	Pearson Correlation Coefficient (R)
1987a Burn	13	0.001	0.786
1987b Burn	11	0.000	0.925
1994a Burn	13	0.075	0.511
1994b Burn	15	0.215	0.340
Unburned Spruce	17	0.827	0.057
All Sites	69	0.001	0.391

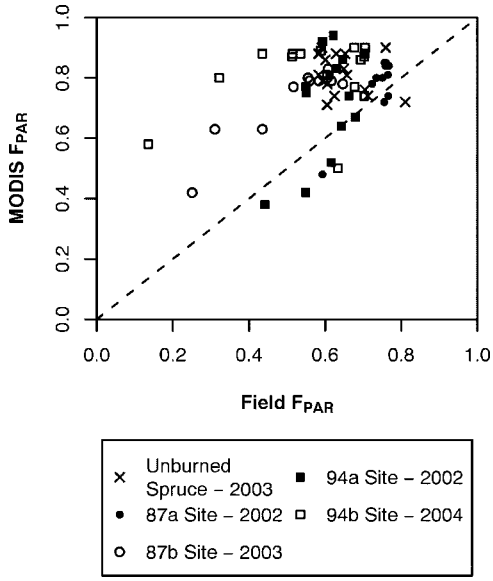

Fig. 8. Comparison of eight-day averages of PAR cell array measurements and eight-day MODIS $\mathrm{F_{PAR}}$ estimates across all sites.

to overestimate the magnitude of $\mathrm{F_{PAR}}$ in these regrowth sites. Timing of green-up and leaf senescence was consistent between the MODIS and field measurements, and the shapes of the seasonal $\mathrm{F_{PAR}}$ curves derived from both were similar. The MODIS product appeared to better capture seasonal changes in $\mathrm{F_{PAR}}$ in deciduous areas where canopy density, and, therefore, $\mathrm{F_{PAR}}$ was greater. We offer a few possible explanations for these observations.

The primary factor affecting differences between MODIS and field measurements was the combination of canopy closure and ground cover vegetation. Ground cover in the region is relatively heterogeneous with most areas dominated by mosses and lichens, or by herbaceous species that exhibit spatial and seasonal changes in density [14]. Because neither the PAR cells nor the ceptometer capture ground cover light interception (just light interception from vegetation greater than $\sim$10 cm in height), in regions where photosynthesizing ground cover is prevalent, field $\mathrm{F_{PAR}}$ values may be lower than those estimated in the MODIS $\mathrm{F_{PAR}}$ product. The MODIS algorithm calculates $\mathrm{F_{PAR}}$ based on reflectance rather than transmittance values and, thus, includes the contribution of ground cover to the total $\mathrm{F_{PAR}}$ signal.

Based on these observations, we would expect to find better agreement between MODIS and PAR cell $\mathrm{F_{PAR}}$ estimates at sites with relatively dense canopies, and, therefore, high $\mathrm{F_{PAR}}$. In these areas, ground cover may be extensive, but because the canopy is dense, the fraction of the total $\mathrm{F_{PAR}}$ signal made up by ground cover is small relative to the fraction made up by the canopy. In contrast, where canopy cover is sparse and ground cover is extensive, the fraction of the total $\mathrm{F_{PAR}}$ signal made up by ground cover will be greater, and, thus, the exclusion of the ground cover component in these areas will have a greater effect than in regions where canopy density is high.

These observations are supported by our results (Figs. 6, 8, and 9). Larger discrepancies between the MODIS and PAR cell measurements were found in areas where low canopy density,

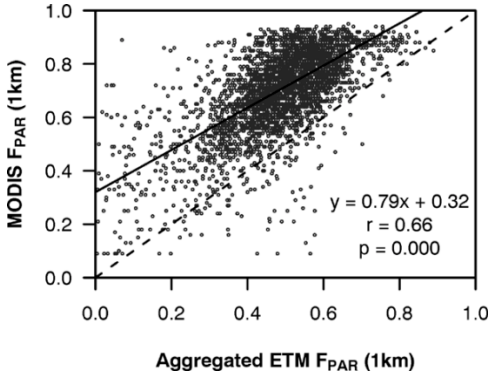

Fig. 9. Comparison of aggregated Landsat F_{PAR} to the MODIS F_{PAR} product at 1-km resolution across the study region.

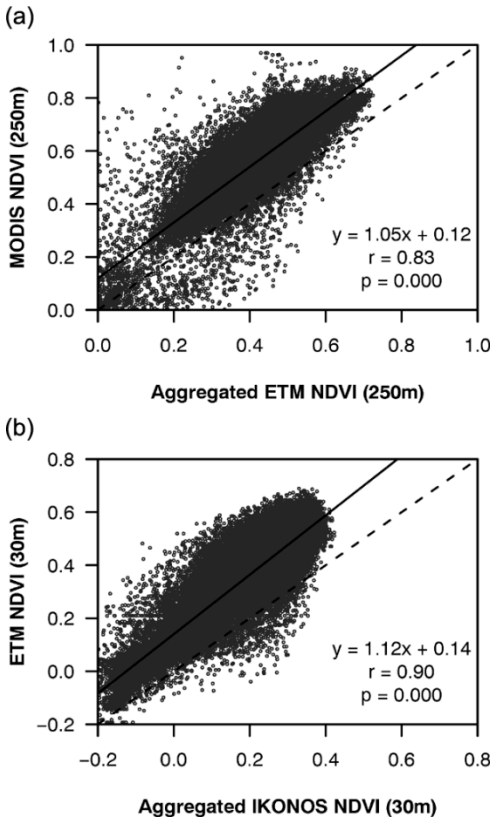

Fig. 10. (a) Comparison of aggregated Landsat NDVI to comparable MODIS 250-m NDVI products across the study region. (b) Comparison of aggregated IKONOS NDVI to the Landsat 30-m NDVI for the area of overlap between both.

and/or prevalent canopy gaps, allowed for more direct influence of ground cover on surface reflectance. Similar results have been noted and modeled in boreal forest and other ecosystems [25]–[28]. The best overall agreement between MODIS and field measurements was found within the 1987 burn, which is characterized by a more uniform canopy, and herbaceous ground cover (see Fig. 2). In contrast, we found greater differences between MODIS and field measurements in the 1994 burn, where canopy density was lower and nonuniform, and ground cover dominated by herbs and mosses. The MODIS product also showed greater seasonal changes in $\mathrm{F_{PAR}}$ relative to field measurements at this site, most likely related to green-up and senescence of ground-cover.

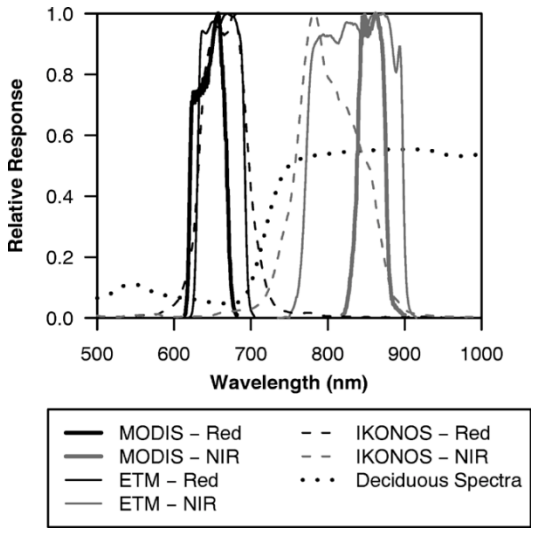

Fig. 11. MODIS-TERRA, Landsat-ETM, and IKONOS spectral response curves for the red and near infrared bands of each sensor.

An effect which could account for some additional disparity between MODIS and the PAR cell measurements, particularly under sparse canopy conditions, is the difference between MODIS F_{PAR} and the ground measurements of intercepted photosynthetically active radiation (F_{IPAR}). Our field measurements did not take into account upwelling or reflected PAR, but the effect of PAR reflectance from the canopy and ground surface on the total F_{PAR} signal is small due to relatively little PAR reflectance from vegetation, subsequent re-absorption by the canopy, and the off-setting effects of PAR reflectance from the canopy and the ground cover. Thus, F_{IPAR} closely approximates F_{APAR}. Differences between the two can occur under sparse canopy conditions [29], [30], but recent field measurements in much sparser Kalahari Woodlands indicate a maximum 4% absolute difference [9].

Another factor accounting for observed differences between MODIS and field F_{PAR} measurements is associated with biome type classification in the MODIS Land Cover product (MOD12Q1). The land cover map separates global vegetation into six distinct biomes: grasses and cereal crops, shrubs, broadleaf crops, savannas, broadleaf forests, and needleleaf forests. Each biome has associated properties describing its structural attributes such as ground cover, vertical heterogeneity, crown, and background brightness. These properties are used to parameterize the three-dimensional radiative transfer model used in the F_{PAR} retrieval algorithm [19]. Biome misclassification may introduce error into the LAI/F_{PAR} solutions, by altering variables accounting for canopy structure, particularly errors associated with the life form composition (i.e. trees versus shrubs or grass) [22], [23]. In the MODIS product, the "savanna" class dominated all burned areas, with needleleaf forest and shrub cover making up the majority of the remaining area. Statistics from the land cover product over the three burned areas indicated that more recent fires had higher percentages of forest cover (Table II), which is not the case in our study area (rather, more recent burns had less tree cover). This observation may be partly associated with charred material being confused with dense evergreen forest cover.

Comparisons of the MODIS F_{PAR} product to high resolution F_{PAR} maps derived from Landsat and the field measurements also indicated that the MODIS product overestimated F_{PAR} relative to Landsat (Fig. 9). This suggests that the differences observed between the field and MODIS F_{PAR} values were not entirely due to scale mismatch between measurements. Spatial heterogeneity within a 1-km MODIS pixel was captured in the aggregated Landsat F_{PAR} maps; thus, we believe scale mismatch was a not primary source of the observed differences. We cannot, however, entirely rule out scale mismatch as a source of error. Although the Landsat images incorporate the influence of ground cover reflectance, the F_{PAR} maps derived from them were based on (i.e., calibrated to) our field measurements, which did not include ground cover contributions to total F_{PAR}. Thus, the Landsat F_{PAR} maps helped to capture and integrate spatial variability in F_{PAR}, but not the ground cover contribution to total F_{PAR} estimated in the MODIS F_{PAR} product. As a result, the absolute magnitudes of the MODIS retrievals were higher than both estimates based on the field measurements, and the higher resolution F_{PAR} maps.

Because maps of F_{PAR} are often generated from empirical relationships with the NDVI, as we have done here and the MODIS algorithm does when a unique F_{PAR} solution is not found, we explored comparisons of the NDVI products as well. The MODIS NDVI product consistently estimated higher NDVI than the aggregated Landsat NDVI (Fig. 10). Similarly, the IKONOS and Landsat NDVI values at the same spatial resolution were highly correlated but offset from one another, with the Landsat systematically higher than IKONOS NDVI across the full range of values. These observations may be the result of differences in sensor bandwidths (Fig. 11) which can alter the NDVI estimated using different sensors not only due to differences in observed in-band surface spectral reflectance, but also as a result of differences in attenuation by various atmospheric constituents. We note that the MODIS NDVI was calculated from reflectance values that were atmospherically corrected [31], whereas the Landsat and IKONOS were not corrected due partly to inadequate atmospheric measurements and partly to its being beyond the scope of our F_{PAR} analysis. Others have noted these NDVI differences between sensors (for example, see [32] and [33]) and demonstrated that absolute atmospheric correction of the in-band reflectances minimizes the NDVI differences observed between sensors [24], [34]. In our case, the Landsat NDVI values, calculated from normalized top-of-atmosphere reflectance, were essentially calibrated to our field F_{PAR} measurements to produce F_{PAR} maps. As such, the NDVI comparisons were not crucial to our F_{PAR} comparisons so long as the relative spatial patterns in NDVI (thus, F_{PAR}) were captured. It is important, however, to consider these NDVI differences in any biophysical retrieval algorithms that rely on multisensor NDVI or surface reflectance values.

VI. Conclusion

MODIS F_{PAR} products were analyzed in a boreal landscape and compared with field F_{PAR} estimates, including a combination of spatially extensive hand-held measurements and a unique

set of continuously operating light sensor arrays. High-resolution F_{PAR} maps were derived from IKONOS and Landsat imagery calibrated to the field measurements. Results indicate that the MODIS F_{PAR} products generally overestimated the magnitude of F_{PAR} relative to both field measurements and high resolution F_{PAR} maps, but captured most of the observed seasonal variability of F_{PAR} (i.e., phenological changes) over the growing seasons for which we had nearly continuous measurements (2002–2004).

Canopy closure and ground cover influences on surface reflectance were the source of at least some of the observed discrepancies between the magnitudes of the F_{PAR} estimates. Differences were most pronounced in more sparsely vegetated areas with denser ground cover (e.g., sites in a 1994 burn regrowth area). In contrast, areas with more uniform canopy cover were better characterized by the MODIS products (e.g., sites in unburned areas and a 1987 burned area). This observation was confirmed by comparisons with the aggregated high-resolution F_{PAR} maps over larger areas than those captured by our field sites.

Related multisensor NDVI comparisons also indicated systematic differences between the MODIS products and the higher resolution sensors used to capture and aggregate spatial variability in F_{PAR}, but we suggest most of these differences were associated with the lack of atmospheric correction of the latter. Our primary purpose for comparing NDVI values was to discern differences in F_{PAR} based on the use of NDVI for empirical F_{PAR} estimation, but our analysis of this was limited to the extent of our field measurements, which did not capture the F_{PAR} of ground cover or vegetation $<$10-cm height. Thus, the high-resolution F_{PAR} maps helped to extend the field measurements and capture spatial variation within the MODIS pixels, but not the absolute magnitude of F_{PAR} beyond the vegetation components measured in the field.

Classification of much of the boreal landscape, particularly burned areas, as a type of savanna in the MODIS land cover product may also influence the MODIS F_{PAR} estimates, as the land cover type is used to prescribe vegetation structural properties used in the algorithm look-up tables. Since the F_{PAR} products are relatively higher order, they also are dependent upon the accuracy of the reflectance and vegetation index products, which are evaluated elsewhere in this special issue. It would be advantageous in future work to attempt to separate errors in F_{PAR} retrievals that result from these various constituents relative to properties of the land surface such as canopy closure and ground cover. The collection 5 (V005) LAI/F_{PAR} product, expected to be in production by the end of 2005 and completed by March of 2007, may address some of the issues in the collection four product outlined in this paper.

The boreal ecosystem is rapidly changing, at least partly due to changes in climate [10], [35], and this is reflected in the dramatic increase in the area burned on an annual basis. It is important that models simulating changes in carbon dynamics, many of which utilize satellite F_{PAR} products, minimize uncertainties associated with the data that drive them while maximizing the factors of interest. Additional validation of F_{PAR} products in a range of environments, including boreal areas associated with fire disturbance, will help to ensure that carbon model results are consistent and robust on annual to inter-annual time scales.

ACKNOWLEDGMENT

The authors would like to thank E. Kasischke, for assistance with field site selection and sampling design, and L. Ferguson, for help with field data collection. They would also like to thank F. Huemmrich and two anonymous reviewers for their constructive comments, as well as the MODIS Land Science Team for their contributions to the production of global data sets.

REFERENCES

[1] P. J. Sellers, R. E. Dickinson, D. A. Randall, A. K. Betts, F. G. Hall, J. A. Berry, C. J. Collatz, A. S. Denning, H. A. Mooney, C. A. Nobre, and N. Sato, "Modeling the exchanges of energy, water, and carbon between the continents and the atmosphere," *Science*, vol. 275, pp. 502–509, 1997.

[2] S. J. Goetz, S. D. Prince, M. M. Thawley, J. Small, and A. Johnston, "Mapping net primary production and related biophysical variables with remote sensing: Application to the BOREAS region," *J. Geophys. Res.*, vol. 104, pp. 27719–27 733, 1999.

[3] S. W. Running, R. R. Nemani, F. A. Heinsch, M. Zhao, M. Reeves, and H. Hashimoto, "A continuous satellite_derived measure of global terrestrial primary production," *BioScience*, vol. 54, pp. 547–560, 2004.

[4] R. B. Myneni, S. Hoffman, Y. Knyazikhin, J. L. Privette, J. Glassy, Y. Tian, Y. Wang, X. Song, Y. Zhang, G. R. Smith, A. Lotsch, M. Friedl, J. T. Morisette, P. Votava, R. R. Nemani, and S. W. Running, "Global products of vegetation leaf area and fraction absorbed PAR from year one of MODIS data," *Remote Sens. Environ.*, vol. 83, pp. 214–241, 2002.

[5] W. B. Cohen and C. O. Justice, "Validating MODIS terrestrial ecology products: Linking *in situ* and satellite measurements," *Remote Sens. Environ.*, vol. 70, pp. 1–3, 1999.

[6] J. T. Morisette, J. L. Privette, and C. O. Justice, "A framework for the validation of MODIS land products," *Remote Sens. Environ.*, vol. 83, pp. 77–96, 2002.

[7] W. Yang, B. Tan, D. Huang, M. Rautiainen, N. V. Shabanov, Y. Wang, J. L. Privette, K. F. Huemmrich, R. Fensholt, I. Sandholt, M. Weiss, R. R. Nemani, Y. Knyazikhin, and R. Myneni, "MODIS leaf area index products: From validation to algorithm improvement," *IEEE Trans. Geosci. Remote Sens.*, vol. 44, no. 7, Jul. 2006.

[8] R. Fensholt, I. Sandhot, and M. S. Rasmussen, "Evaluation of MODIS LAI, fAPAR and the relation between fAPAR and NDVI in a semi-arid environment using *in situ* measurements," *Remote Sens. Environ.*, vol. 91, pp. 490–507, 2004.

[9] K. F. Huemmrich, J. L. Privette, M. Mukelabai, R. B. Myneni, and Y. Knyazikhin, "Time-series validation of MODIS land biophysical products in a Kalahari woodland, Africa," *Int. J. Remote Sens.*, to be published.

[10] ACIA (Arctic Climate Impact Assessment). (2004) Impacts of a Warming Arctic: Arctic Climate Impact Assessment. Cambridge University Press. [Online]. Available: http://www.acia.uaf.edu

[11] C. O. Justice, J. R. Townshend, E. F. Vermote, E. Masuoka, R. E. Wolfe, N. Saleous, D. P. Roy, and J. T. Morisette, "An overview of MODIS Land data processing and product status," *Remote Sens. Environ.*, vol. 83, pp. 3–15, 2002.

[12] A. D. McGuire, S. Sitch, and U. Wittenberg, "Carbon balance of the terrestrial biosphere in the twentieth century: Analyses of CO2, climate, and land use effects with four process-based ecosystem models," *Global Biogeochem. Cycles*, vol. 15, pp. 183–206, 2001.

[13] J. M. Chen, W. Ju, J. Cihlar, D. Price, J. Liu, W. Chen, J. Pan, T. A. Black, and A. Barr, "Spatial distribution of carbon sources and sinks in Canada's forests based on remote sensing," *Tellus B*, vol. 55, pp. 622–642, 2003.

[14] M. T. Jorgenson, J. E. Roth, M. D. Smith, S. Schlentner, W. Lentz, E. R. Pullman, and C. H. Racine, *An Ecological Land Survey for Fort Greely, Alaska*. Hanover, NH: U.S. Army Corps Eng. Cold Regions Res. Eng. Lab., 2001.

[15] M. C. Mack, K. Treseder, K. Manies, J. Harden, T. Schuur, J. T. Randerson, and S. Chapin, "Effects of fire and plant species composition on plant biomass, carbon and nitrogen pools and aboveground NPP in interior Alaska," *Agr. Forest Meteorol.*, to be published.

[16] E. Hyer and S. Goetz, "Comparison and sensitivity analysis of instruments and radiometric methods for LAI estimation: Assessments from a boreal forest site," *Agr. Forest Meteorol.*, vol. 122, pp. 157–174, 2004.
[17] J. M. Norman and G. S. Campbell, "Canopy structure," in *Plant Physiological Ecology: Field Methods and Instrumentation*, R. W. Pearcy, J. Ehleringer, H. A. Mooney, and P. W. Rundel, Eds. London, U.K.: Chapman & Hall, 1989, pp. 301–325.
[18] Y. Knyazikhin, J. V. Martonchik, R. B. Myneni, D. J. Diner, and S. W. Running, "Synergistic algorithm for estimating vegetation canopy leaf area index and fraction of absorbed photosynthetically active radiation from MODIS and MISR data," *J. Geosci. Res. Atmos.*, vol. 103, pp. 32 257–32 275, 1998.
[19] Y. Knyazikhin, J. Glassy, J. L. Privette, Y. Tian, A. Lotsch, Y. Zhang, Y. Wang, J. T. Morisette, P. Votava, R. B. Myneni, R. R. Nemani, and S. W. Running. (1999, April) MODIS Leaf Area Index (LAI) and Fraction of Photosynthetically Active Radiation Absorbed by Vegetation (FPAR) Product (MOD15) Algorithm Theoretical Basis Document. [Online]. Available: http://eospso.gsfc.nasa.gov/atbd/modistables.html
[20] A. Strahler, D. Muchoney, J. Borak, M. Friedl, S. Gopal, E. Lambin, and A. Moody. (1999) MODIS Land Cover Product Algorithm Theoretical Basis Document, Version 5: MODIS Land Cover and Land Cover Change. [Online]. Available: http://modis.gsfc.nasa.gov/data/atbd/atbd_mod12.pdf
[21] A. Huete, C. Justice, and W. Leeuwen. (1999) *MODIS Vegetation Index (MOD 13) Algorithm Theoretical Basis Document* [Online]http://modis.gsfc.nasa.gov/data/atbd/atbd_mod13.pdf
[22] Y. Tian, Y. Zhang, Y. Knyazikhin, J. Bogaert, and R. B. Myneni, "Prototyping of MODIS LAI and FPAR algorithm with LASUR and LANDSAT data," *IEEE Trans. Geosci. Remote Sens.*, vol. 38, no. 5, pp. 2387–2401, Sep. 2000.
[23] A. Lotsch, Y. Tian, M. A. Friedl, and R. B. Myneni, "Land cover mapping in support of LAI and FPAR retrievals from EOS-MODIS and MISR: Classification methods and sensitivities to errors," *Int. J. Remote Sens.*, vol. 24, pp. 1997–2016, 2003.
[24] S. J. Goetz, "Multi-sensor analysis of NDVI, surface temperature and biophysical variables at a mixed grassland site," *Int. J. Remote Sens.*, vol. 18, pp. 71–94, 1997.
[25] S. J. Goetz and S. D. Prince, "Remote sensing of net primary production in boreal forest stands," *Agr. Forest Meteorol.*, vol. 78, pp. 149–179, 1996.
[26] J. Chen, "Canopy architecture and remote sensing of the fraction of photosynthetically active radiation absorbed by boreal forest conifers," *IEEE Trans. Geosci. Remote Sens.*, vol. 34, no. 6, pp. 1353–1368, Nov. 1996.
[27] N. Goel and W. Qin, "Influence of canopy architecture on various vegetation indices and LAI and FPAR: Simulation model results," *Remote Sens. Rev.*, vol. 10, pp. 309–347, 1994.
[28] N. V. Shabanov, Y. Wang, W. Buermann, J. Dong, S. Hoffman, G. R. Smith, Y. Tian, Y. Knyazikhin, and R. B. Myneni, "Effect of foliage spatial heterogeneity in the MODIS LAI and FPAR algorithm over broadleaf forests," *Remote Sens. Environ.*, vol. 85, pp. 410–423, 2003.
[29] S. D. Prince, "A model of regional primary production for use with coarse resolution satellite data," *Int. J. Remote Sens.*, vol. 12, pp. 1313–1330, 1991.
[30] K. F. Huemmrich and S. N. Goward, "Vegetation canopy PAR absorptance and NDVI: An assessment for ten tree species with the SAIL model," *Remote Sens. Environ.*, vol. 61, pp. 254–269, 1997.
[31] E. F. Vermote, N. Z. El Saleous, and C. O. Justice, "Atmospheric correction of MODIS data in the visible to middle infrared: First results," *Remote Sens. Environ.*, vol. 83, pp. 97–111, 2002.
[32] M. D. Steven, T. J. Malthus, F. Baret, H. Xu, and M. J. Chopping, "Intercalibration of vegetation indices from different sensor systems," *Remote Sens. Environ.*, vol. 88, pp. 412–422, 2003.
[33] S. N. Goward, P. E. Davis, D. Fleming, L. Miller, and J. R. Townshend, "Empirical comparison of Landsat 7 and IKONOS multispectral measurements for selected Earth Observation System (EOS) validation sites," *Remote Sens. Environ.*, vol. 88, pp. 80–99, 2003.
[34] M. Pagnutti, K. Holekamp, R. E. Ryan, R. D. Vaughan, J. A. Russel, D. Prados, and T. Stanley, "Atmospheric correction of high spatial resolution commercial satellite imagery products using MODIS atmospheric products," in *Proc. Int. Workshop on the Analysis of Multi-Temporal Remote Sensing Images*, 2005, pp. 115–119.
[35] S. J. Goetz, A. Bunn, G. Fiske, and R. A. Houghton, "Satellite observed photosynthetic trends across boreal North America associated with climate and fire disturbance," *Proc. Nat. Acad. Sci.*, vol. 102, pp. 13 521–13 525, 2005.

Daniel C. Steinberg received the B.A. degree in earth and atmospheric sciences from Cornell University, Ithaca, NY, in 2004.

His interests are focused on the use of satellite remote sensing and GIS techniques for monitoring and understanding the effects of climatic disruption on carbon cycling, biodiversity, and human health. During his undergraduate career, he worked within the Ocean Resources and Ecosystems Program in the Center for the Environment, Cornell University, where he investigated biological responses to climate variability in marine environments. He has been a Research Assistant at the Toolik Long Term Ecological Research site in Alaska and has interned at the Marine Biological Laboratory, Woods Hole, MA. Currently, he is with the Woods Hole Research Center, where he focuses on the use of satellite imagery and GIS to inform models of carbon uptake by vegetation in boreal and temperate forests.

Scott J. Goetz received the B.S. degree from Pennsylvania State University, State College, the M.S. degree from the University of California, Santa Barbara, and the Ph.D. degree from the University of Maryland, College Park.

He works on the application of satellite imagery to analyses of environmental change, including monitoring and modeling links between land use change of various types (e.g., urbanization, fire disturbance), forest productivity, water quality, biological diversity, and disease vectors. Before joining the Woods Hole Research Center, Woods Hole, MA, in 2003, where he is now a Senior Scientist, he was on the Faculty at the University of Maryland, College Park, for seven years, where he maintains an Adjunct Associate Professor appointment. He was a Research Scientist for various contractors at the NASA Goddard Space Flight Center from 1985 to 1995. He has authored, to date, over 50 refereed journal publications and book chapters, and recently edited a special issue on advances in biophysical remote sensing.

Dr. Goetz serves on the editorial board of *Remote Sensing of Environment*.

Edward J. Hyer received the B.A. degree in chemistry from Goucher College, Towson, MD, the M.A. degree from the University of Lisbon, Lisbon, Portugal, and the Ph.D. degree in geography for his dissertation entitled "Investigating uncertainties in trace gas emissions from boreal forest fires using MOPITT measurements of carbon monoxide and a global chemical transport model" from the University of Maryland, College Park, in 1992, 2002, and 2005, respectively, all in geography.

He has been involved in projects dealing with a diverse range of issues related to ecosystem function and carbon cycling in the boreal forest. During his time as a graduate student, he was involved in field and modeling investigations of wildfire carbon emissions, canopy light interception, and soil moisture dynamics. He is now with the Marine Meteorology Division, Naval Research Laboratory (NRL), Monterey, CA. His work at NRL will apply lessons from his dissertation research to broader issues in emissions modeling and pollution forecasting, while maintaining his involvement in boreal ecology research.